Front. Optoelectron. 2020, 13(3): 256–264
https://doi.org/10.1007/s12200-020-1013-3

RESEARCH ARTICLE

Influence of precursor concentration on printable mesoscopic perovskite solar cells

Shuangquan JIANG*, Yusong SHENG*, Yue HU, Yaoguang RONG, Anyi MEI (✉), Hongwei HAN

Michael Grätzel Center for Mesoscopic Solar Cells, Wuhan National Laboratory for Optoelectronics, Huazhong University of Science and Technology, Wuhan 430074, China

Abstract Over the last decade, the power conversion efficiency of hybrid organic–inorganic perovskite solar cells (PSCs) has increased dramatically from 3.8% to 25.2%. This rapid progress has been possible due to the accurate control of the morphology and crystallinity of solution-processed perovskites, which are significantly affected by the concentration of the precursor used. This study explores the influence of precursor concentrations on the performance of printable hole-conductor-free mesoscopic PSCs via a simple one-step drop-coating method. The results reveal that lower concentrations lead to larger grains with inferior pore filling, while higher concentrations result in smaller grains with improved pore filling. Among concentrations ranging from 0.24–1.20 M[1)], devices based on a moderate strength of 0.70 M were confirmed to exhibit the best efficiency at 16.32%.

Keywords printable perovskite solar cell (PSC), precursor concentration, crystallization, morphology

1 Introduction

Over the past decade, perovskite solar cells (PSCs) have been the focus of much research [1–8]. The record-certified power conversion efficiency (PCE) of PSCs has increased rapidly to 25.2%, rivaling the optimum efficiency of silicon-based solar cells [2]. This rapid increase in efficiency is largely attributed to the improved control of the crystallinity and morphology of halide perovskites, which generally have the formula of ABX_3, where A is a monovalent cation, such as methylammonium (MA^+); B is a divalent metal, such as lead (Pb^{2+}); and X is a halogen anion, such as iodide (I^-) [9–11]. Generally, properties of good crystallinity, such as large grain size, along with well-developed orientation are required for inhibiting non-radiative recombination and promoting charge-carrier transport in halide perovskite films [12,13]. Additionally, morphological preferences, such as good uniformity and effective coverage, are essential for absorbing light and inhibiting shunt caused by undesired contact between the other layers in PSCs [12,13].

Since halide perovskites are solution-processable, most PSCs are currently prepared via solution-processed methods [2]. The composition of the precursor is fundamental in the processing of solutions [14,15]. For example, the precursor of $MAPbI_3$ is usually prepared by directly dissolving methylammonium iodide (MAI) and lead iodide (PbI_2) in selected solvents, such as dimethylformamide (DMF) or γ-butyrolactone (GBL) [16–18]. An intensive study on the precursor of $MAPbI_3$ revealed that the precursor is not a pure solution; since a typical Tyndall effect is easily observed when a laser passes through the precursor, it can be defined as somewhat colloidal [19]. These colloidal precursor particles can be as large as 1 μm [19]. In the crystallization process of halide perovskites from their precursors, the existing colloidal particles function as nucleation sites during film preparation, thereby influencing the quality of the obtained films [12,13]. Additionally, the colloidal nature of the precursor is influenced by its concentration; a lower concentration can help to promote the precursor to a real solution [19]. Therefore, the concentration of the precursor is fundamental for controlling both the crystallinity and morphology of halide perovskites.

The influence of precursor concentrations has been demonstrated via the sequential deposition method in

Received February 8, 2020; accepted April 28, 2020

E-mail: anyimei@hust.edu.cn

*These authors contributed equally.

1) 1 M = 1 mol/L

which PbI_2 is spin-coated and MAI is introduced after [20]. Bi et al. confirmed that for the preparation of perovskite films with good crystallinity and morphology, a moderate PbI_2 concentration of 1.0 M is the most appropriate [21]. They found that a 1.0-M precursor resulted in an efficiency of 13.99%, while an efficiency of 1.4% was obtained at a concentration of 0.1 M. Zhang et al. discovered that a high MAI concentration is beneficial for obtaining high-quality perovskite films [22]. In their study, MAI at a concentration of 8 mg/mL resulted in an efficiency of 7.46%, while a concentration of 15 mg/mL produced an efficiency of 12.76%. Furthermore, the influence of precursor concentration has also been demonstrated in the antisolvent method [17], in which an antisolvent is dripped during the spin-coating of the precursor. Wieghold et al. confirmed that larger and more oriented grains resulted from higher precursor concentrations [23].

However, research is currently lacking on the impact of precursor concentration in a simple one-step drop-coating method [24,25]. This approach is generally applied in the fabrication of printable mesoscopic hole-conductor-free PSCs (PMPSCs). PMPSCs comprise a printed porous $TiO_2/ZrO_2/C$ triple layer filled with halide perovskites and are a particular type of PSC [26]. When used together with C electrodes, the application of these devices is seen as commercially promising in terms of low cost and improved stability [27]. PMPSC efficiency is dependent on the control of the crystallinity and morphology of halide perovskites in the porous structure. The crystallization process in a simple one-step drop-coating method is different from both the sequential deposition approach and the antisolvent method since the simple drop-coating method involves a much slower crystallization process. Therefore, studying the influence of precursor concentrations in the simple one-step drop-coating method is important for the successful development of PMPSCs.

This study investigates the influence of precursor concentrations between 0.24–1.20 M on the crystallinity and morphology of drop-coated $MAPbI_3$ perovskites and explores their impact on the performance of printable mesoscopic hole-conductor-free PSCs. It is demonstrated that a lower concentration of 0.24 M leads to the formation of larger grains, while better coverage is obtained with a higher concentration of 1.20 M. In terms of device performance, a moderate concentration of 0.70 M produces the highest efficiency of 16.32%, 0.24 M leads to an efficiency of 15.38%, while a concentration of 1.20 M produces an efficiency of 15.89%.

2 Experimental section

Materials PbI_2 and MAI were obtained from p-OLED, and 5-Ammonium valeric acid iodide (5-AVAI) was sourced from Shanghai MaterWin New Materials Co., Ltd. Sigma-Aldrich provided the GBL, and ethanol was obtained from Sinopharm Chemical Reagent Co., Ltd. The pastes for the mesoscopic layers were sourced from WonderSolar Co., Ltd. All materials were used as received without further purification.

Precursor preparation The $MAPbI_3$ precursor with a concentration of 1.2 M and additional 5-AVAI was prepared by dissolving 1.5362-g MAI, 0.0828-g 5-AVAI, and 4.61-g PbI_2 in 8.3 mL of mixed solvent containing GBL and ethanol (9:1 volume ratio) [28]. The other concentrations of 0.24, 0.41, 0.55, 0.70, 0.83, and 1.00 M were obtained by diluting 1.2 M of precursor with the mixed solvent.

Device fabrication The fluorine-doped tin oxide (FTO) glasses were laser-etched with the desired patterns and were cleaned by ultrasonication in water with detergent, deionized water, and ethanol, respectively. A compact layer of TiO_2 (c-TiO_2) was then deposited on the FTO glass by spray pyrolysis at 450°C. This was followed by the screen printing and annealing of the porous TiO_2 (mp-TiO_2) layer (700 nm, annealed at 500°C), the ZrO_2 mp-TiO_2 layer (3 μm, annealed at 500°C), and the C layer (10 μm, annealed at 400°C). After cooling to room temperature, a simple one-step drop-coating method infiltrated the precursor into the porous $TiO_2/ZrO_2/C$ scaffold. After slow drying at 50°C, printable hole-conductor-free mesoscopic PSCs were obtained.

Characterization A field-emission scanning electron microscope (SEM) (Nova NanoSEM 450) was used to obtain both top-view SEM images of the perovskite-infiltrated porous ZrO_2 layers and cross-sectional images of the devices. The ultraviolet–visible (UV–Vis) spectra were measured using a PerkinElmer Lambda 950 spectrophotometer. Time-resolved photoluminescence (TRPL) decay transients were measured with a Horiba Jobin Yvon FluoroMax-4 fluorimeter. X-ray diffraction (XRD) measurements were obtained using an X'Pert PRO X-ray diffractometer. The incident photon conversion efficiency (IPCE) was measured using a 150-W xenon lamp (Oriel) fitted with a monochromator (Cornerstone 74004) as a monochromatic light source. Photocurrent density–voltage (J–V) curves of both reverse scan (1.2 to −0.2 V) and forward scan (−0.2 to 1.2 V) together with steady outputs were characterized with a Keithley 2400 source/meter and a Newport solar simulator providing light with a spectral distribution of AM 1.5 G. A black mask with a circular aperture of 0.1 cm^2 was applied on top of the cell.

3 Results and discussion

Figure 1 presents the top-view SEM images of drop-coated perovskite films formed from precursors of different concentrations on porous ZrO_2 layers. At a concentration as low as 0.24 M, the ZrO_2 layer is partially covered by perovskite films with distinguishable bare areas (Fig. 1(a)). Coverage improves as the concentration increases, and at

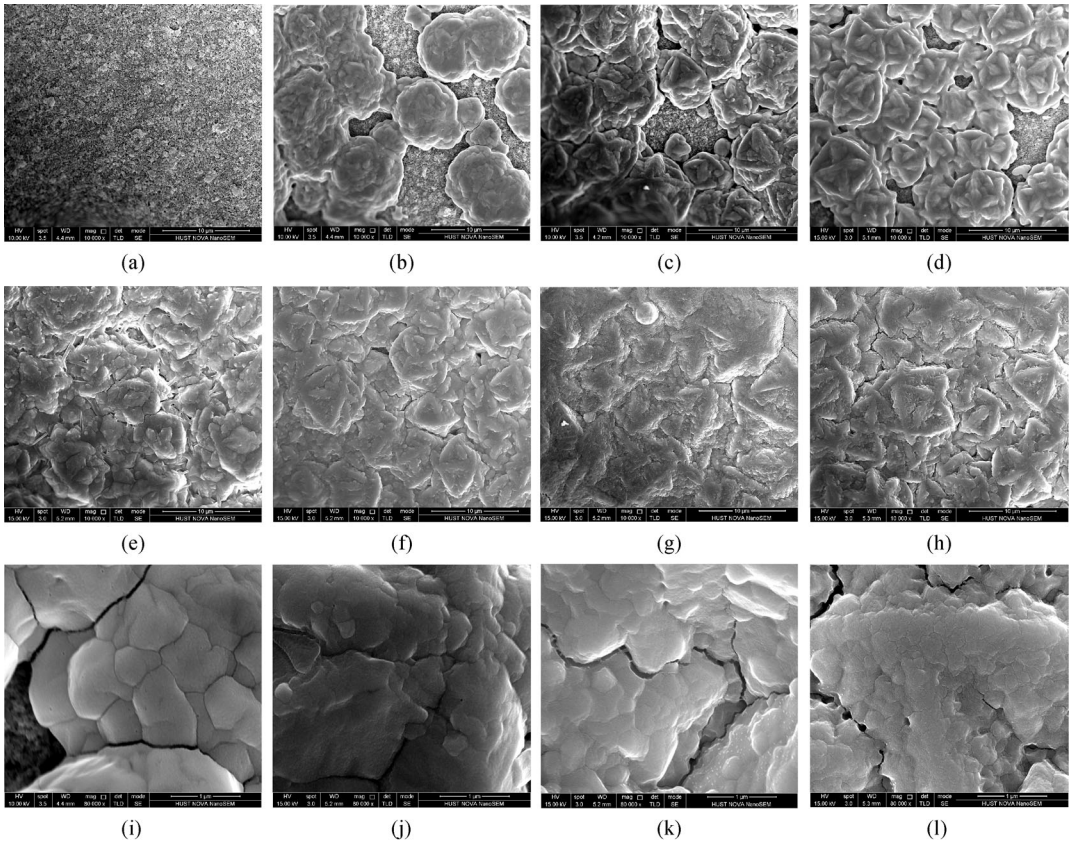

Fig. 1 Top-view SEM images of drop-coated perovskite films on a porous ZrO_2 layer with different precursor concentrations at 10000× magnification: (a) bare ZrO_2, (b) 0.24, (c) 0.41, (d) 0.55, (e) 0.70, (f) 0.83, (g) 1.00, and (h) 1.20 M concentrations. At 80000× magnification: (i) 0.24, (j) 0.70, (k) 0.83, and (l) 1.20 M concentrations

concentrations of 0.7 M and above, complete coverage is achieved. SEM images with higher magnification of films obtained from precursors at concentrations of 0.24, 0.70, 0.83, and 1.20 M were also acquired (as shown in Figs. 1(i)–1(l); they reveal that the perovskite domains consist of small grains. The grain sizes in the films from the 0.24-M precursor are noticeably larger than those obtained from the 1.20-M precursor.

The perovskite's crystallization process from the precursor in the porous substrate is complicated and involves three probable nucleation processes: the inducement of heterogeneous nucleation by the substrate, the inducement of heterogeneous nucleation by colloidal particles in the precursor, and the inducement of homogeneous nucleation by the real solution portion of the precursor. Since the crystallization process of the simple drop-coating method is quite slow, homogeneous nucleation is not dominant. Therefore, the crystallization process is determined by both the substrate and the colloidal properties of the precursor.

Considering that substrates are identical, the variations in coverage mainly result from different crystallization processes induced by varying precursor concentrations. During the annealing process, there is fast precipitation of large colloidal particles in precursors with higher concentrations that results in the uniform distribution of multiple nucleation site on the substrates. Consequently, the perovskite films are continuous and provide good substrate coverage. At low concentrations, there are too few nucleation sites to provide good substrate coverage, and the crystallization process is slower. The slow removal of solvent at 50°C during annealing results in larger-sized grains. This process differs from the spin-coating methods used for preparing perovskite films in which the crystallization process is generally quite fast, and the growth time of the grains is quite short. However, although the 0.24-M precursor results in larger grain sizes, they are not large enough to connect together to form a continuous perovskite film.

Consequently, the authors suggest that if the number of nucleation sites can be reduced, and the crystallization process can be optimized by inhibiting the colloidal nature of the precursor via appropriate control, the method of establishing continuous and uniform perovskite films with larger grain sizes by optimizing precursor concentrations is promising.

Figure 2(a) presents the XRD patterns of perovskite films prepared on porous ZrO_2 layers. At different precursor concentrations, the XRD patterns exhibit a similar form with strong diffraction peaks at 14.02°,

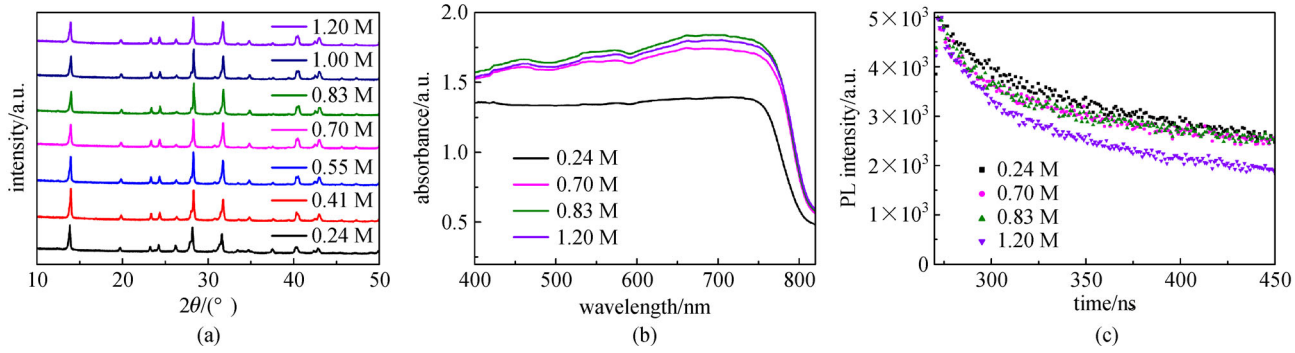

Fig. 2 Optical characterization of drop-coated perovskite films on a porous ZrO_2 layer: (a) XRD patterns, (b) UV–Vis spectra, and (c) TRPL spectra of drop-coated perovskite films on a porous ZrO_2 layer

19.92°, 28.32°, 31.76°, 40.46°, and 43.02°; these can be accurately indexed as crystal faces at (110), (112), (220), (310), (224), and (314). However, the results for light absorption reveal significant differences. As shown in the UV–Vis absorption spectra in Fig. 2(b), the absorbance of the film prepared with the 0.24-M precursor is much lower than those films prepared with precursors at higher concentrations. As discussed in Fig. 1, those films prepared with the 0.24-M precursor contain many bare areas, which signifies insufficient light absorption. Conversely, those continuous films prepared with higher concentration precursors result in stronger absorption.

This study also examined the carrier lifetimes in different perovskite films using TRPL measurements (Fig. 2(c)). The carrier lifetime in films prepared from a precursor of 0.24 M is clearly longer than in those films prepared from a precursor of 1.20 M. This indicates that low precursor concentrations lead to perovskite films with fewer defects. This effect is likely to be attributed to the enlarged grain size.

To clarify the influence of precursor concentrations on device performance, this study fabricated printable hole-conductor-free mesoscopic PSCs. Figure 3(a) presents the PMPSCs in schematic form. PMPSCs comprise an FTO glass and a printed porous $TiO_2/ZrO_2/C$ triple layer. After drop coating, perovskite infiltrates the porous triple layer and grows inside. Figure 3(b) is a typical cross-sectional SEM image of a PMPSC. Generally, the porous TiO_2 layer is about 700 nm thick, the porous ZrO_2 layer is about 3 μm in thickness, and the thickness of the C layer is about 10 μm. Figure 3(c) shows the energy-level alignment in the device. TiO_2 serves as an electron collection and transportation layer, C serves as the back electrode and collects holes, and ZrO_2 functions as a spacer to inhibit recombination by separating TiO_2 and C. Perovskite serves as the light absorber. Since no additional hole-transport materials are applied in PMPSCs, perovskite also serves as the hole conductor.

Figure 3(d) contains the current *J–V* curves of the reverse scan (from open circuit to short circuit) corresponding to the peak efficiency of PMPSCs filled with precursors of different concentrations. These curves are relatively concentrated, signifying minimal variation in peak efficiency. This is quite different from the reported results that indicate wide variations in the efficiency of PSCs prepared with low- and high-concentration precursors. This could be attributed to structural differences in devices or in perovskite preparation methods. Due to the ZrO_2 layer in PMPSCs, non-continuous perovskite will not allow direct contact between the top and bottom layers. Additionally, the thick porous layer also aids light absorption. Furthermore, the slow crystallization process can, to some extent, ensure the crystallinity and morphology of perovskite.

Detailed parameters of the *J–V* curves (reverse scan from the short to the open circuit) together with the forward scan (from the open to the short circuit) performance parameters are presented in Table 1. The efficiencies of the reverse scan for PMPSCs obtained from different precursor concentrations of 0.24, 0.41, 0.55, 0.70, 0.83, 1.00, and 1.20 M are 14.29%, 14.84%, 15.11%, 15.31%, 15.06%, 14.85%, and 14.83%, respectively. The highest efficiency is obtained at a moderate concentration of 0.70 M. The efficiencies from the forward scan are 15.38%, 15.67%, 16.00%, 16.32%, 16.12%, 16.09%, and 15.89%, respectively. The highest efficiency obtained is 16.32%. The efficiency of the forward scan is evidently larger than that of the reverse scan, indicating an abnormal hysteresis phenomenon [29,30]. Previous research has demonstrated that this phenomenon is related to both charge accumulation and imbalanced charge extraction. To obtain an accurate PCE under conditions of hysteresis, a steady-state current density output under a given voltage bias from a maximum power point was conducted. The steady-state current density output results of those PMPSCs prepared with precursors of different concentrations are shown in Fig. 3(e). The calculated steady efficiencies are 14.35%, 14.65%, 15.09%, 15.35%, 15.16%, 14.98%, and 14.82%, respectively, which are similar to the efficiency values obtained by the reverse scan. It is evident from the steady-

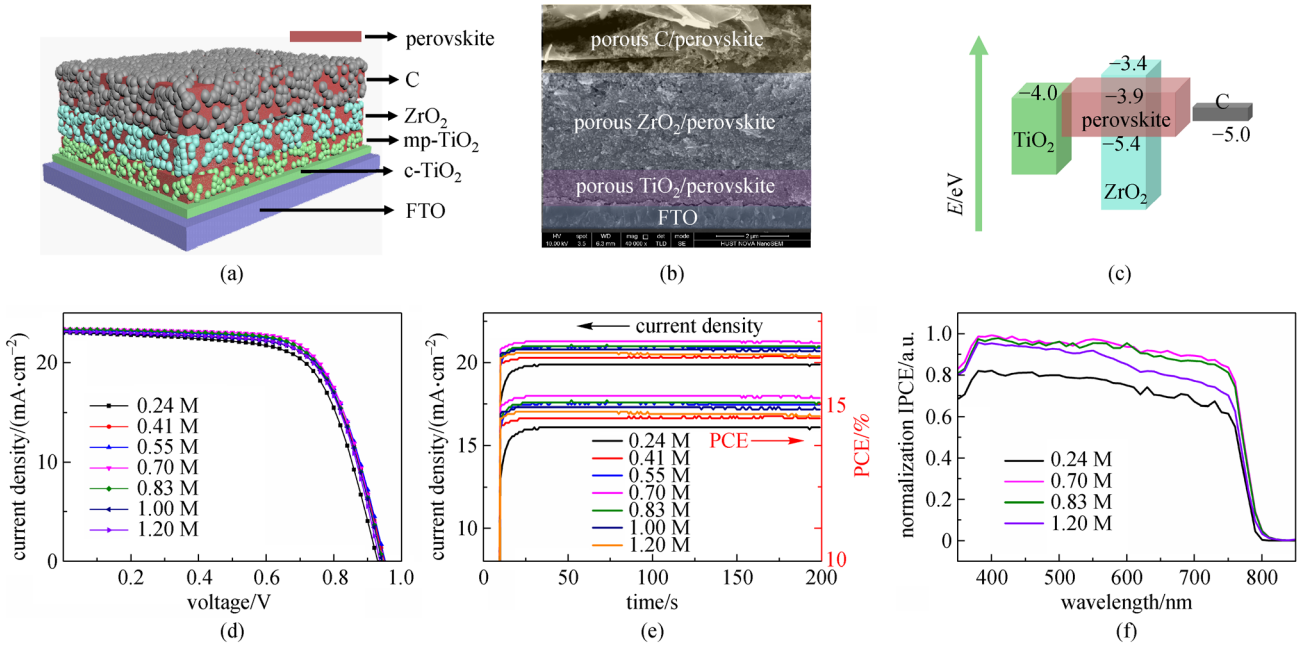

Fig. 3 (a) Schematic, (b) typical cross-sectional SEM image, (c) energy-level alignment of PMPSCs, (d) *J*–*V* curves, (e) steady-state current density output, and (f) IPCE of PMPSCs filled with perovskite precursors at different concentrations

Table 1 *J*–*V* parameters and steady-state outputs of PMPSCs prepared with precursors of different concentrations

	scan direction	V_{OC}/V	J_{SC}/(mA·cm^{-2})	FF	PCE/%	steady-state current density /(mA·cm^{-2})	bias voltage/V	steady-state PCE/%
0.24 M	reverse	0.92	23.00	0.68	14.29	19.93	0.72	14.35
	forward	0.96	22.91	0.70	15.38			
0.41 M	reverse	0.94	23.10	0.68	14.84	20.35	0.72	14.65
	forward	0.98	23.04	0.69	15.67			
0.55 M	reverse	0.96	23.23	0.68	15.11	20.96	0.72	15.09
	forward	0.98	23.20	0.70	16.00			
0.70 M	reverse	0.94	23.39	0.70	15.31	21.32	0.72	15.35
	forward	0.96	23.32	0.73	16.32			
0.83 M	reverse	0.94	23.31	0.69	15.06	21.05	0.72	15.16
	forward	0.96	23.26	0.72	16.12			
1.00 M	reverse	0.94	23.04	0.69	14.85	20.81	0.72	14.98
	forward	0.98	22.93	0.72	16.09			
1.20 M	reverse	0.94	23.10	0.68	14.83	20.59	0.72	14.82
	forward	0.96	23.02	0.72	15.89			

state current density that a low concentration of 0.24 M and a high concentration of 1.20 M lead to a lower current density than the moderate concentration of 0.7 M. This finding is consistent with the trend shown by the IPCE results in Fig. 3(f). At a low concentration of 0.24 M, the IPCE is lower due to insufficient pore filling. At a high concentration of 1.20 M, the device demonstrates a quicker drop of photon conversion efficiency in the band of 550–800 nm. This is probably due to the inability of smaller grains induced by higher concentrations to effectively absorb long-wavelength photons.

This study also fabricated batches of PMPSCs to further verify the results of the influence of concentration on PMPSC performance. The statistical results are presented in Fig. 4. The open circuit voltage (V_{OC}) trend varies little with concentration, except at 0.24 M. As the concentration

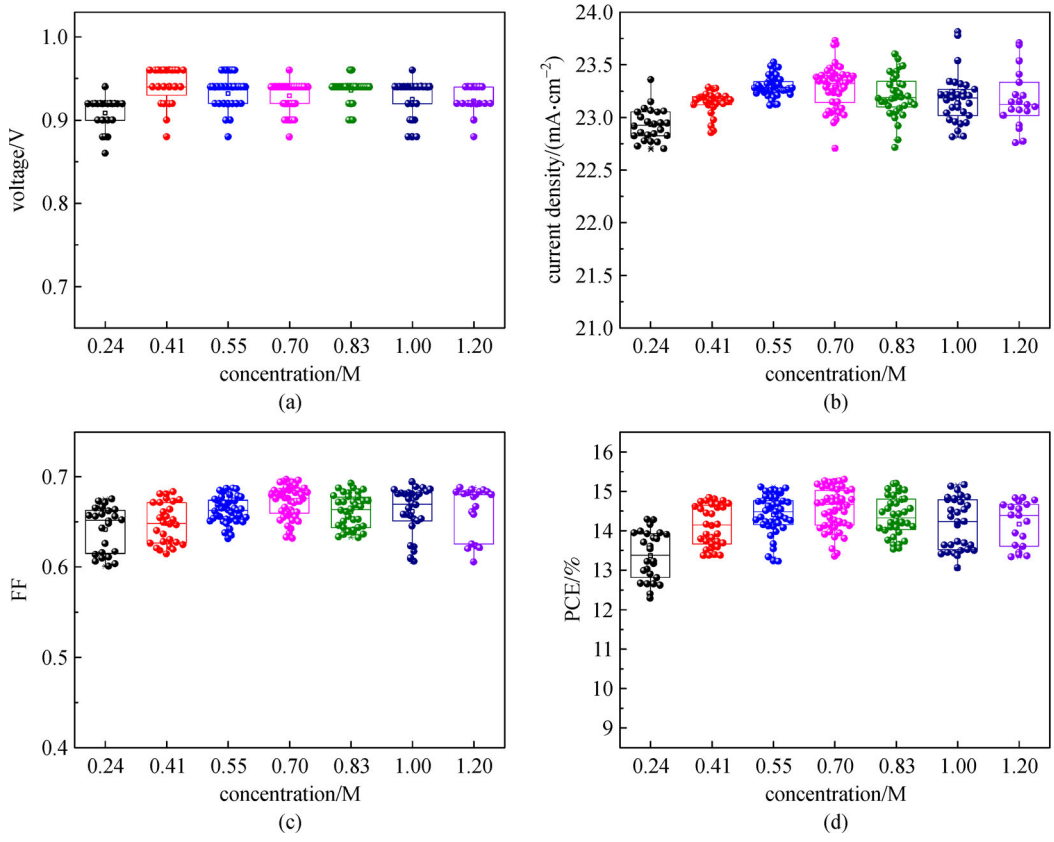

Fig. 4 Statistical results of the performance of PMPSCs filled with perovskite precursors of different concentrations: (a) V_{OC}, (b) J_{SC}, (c) FF, and (d) PCE

increases, the short circuit current density (J_{SC}) initially increases and then decreases. A concentration of 0.70 M results in improved J_{SC}. Additionally, the fill factor (FF) also changes with concentration, and the optimum result is achieved at 0.70 M; consequently, the optimum efficiency is obtained with 0.70 M. The resulting statistical PCE trend is consistent with that determined from the peak efficiency.

Figures 5(a)–5(c) are the cross-sectional SEM images of PMPSCs filled with 0.24, 0.70, and 1.20-M perovskite precursors. The performance of PMPSCs is determined by the perovskite filling in the triple layer. As shown in the areas marked by dashed lines in Fig. 5(a), it is evident that the pores are not well filled, indicating the existence of non-continuous perovskite. Both light absorption and charge transport are restricted by these unfilled areas, resulting in lower J_{SC} and FF values. Insufficient pore filling could also result in poor contact between perovskite and C or TiO_2, which affects the V_{OC}. Therefore, the efficiency of devices filled with 0.24-M perovskite is relatively poor. The filling at a concentration of 1.20 M is much better than that at 0.24 M. However, there remain multiple areas that are poorly filled. This is likely to be attributed to the rapid speed of the crystallization process from high-concentration precursors, which results in some pores not being filled in time. These unfilled areas may also induce recombination and affect light absorption, further restricting performance. At a concentration of 0.70 M, the device has a fairly compact cross section, indicating effective pore filling. This adequate filling and the superior crystallinity of halide perovskites ensure sufficient light absorption and charge-carrier transport, resulting in PMPSCs with optimum efficiency.

This study further applied the optimized concentration of 0.70 M to fabricate additional PMPSCs. By adjusting the thickness of the triple layer, devices with smaller hysteresis were obtained. A typical optimized device exhibited a reverse-scan efficiency of 15.86% with a V_{OC} of 0.94 V, a J_{SC} of 23.42 mA/cm^2, and an FF of 0.72; the device produced a forward scan efficiency of 15.99% with a V_{OC} of 0.96 V, a J_{SC} of 23.33 mA/cm^2, and an FF of 0.71 (Fig. 6). The authors' previous study revealed that the thickness of the compact layer significantly influences the hysteresis of PMPSCs [29]. Therefore, a detailed investigation of the influence of other layers on the hysteresis of PMPSCs would be an appropriate area for future research.

4 Conclusions

This study investigated the influence of precursor concentration on the crystallinity and morphology of halide perovskites prepared by a simple drop-coating

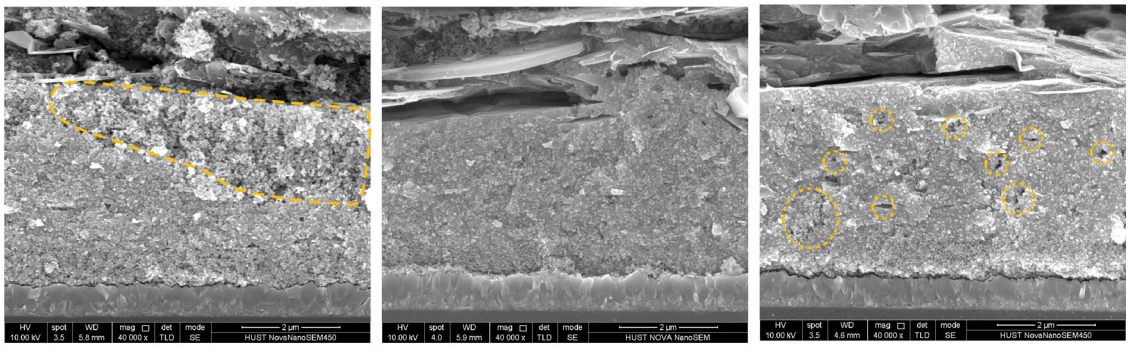

Fig. 5 Cross-sectional SEM images of PMPSCs filled with perovskite precursors of different concentrations: (a) 0.24, (b) 0.70, and (c) 1.20 M

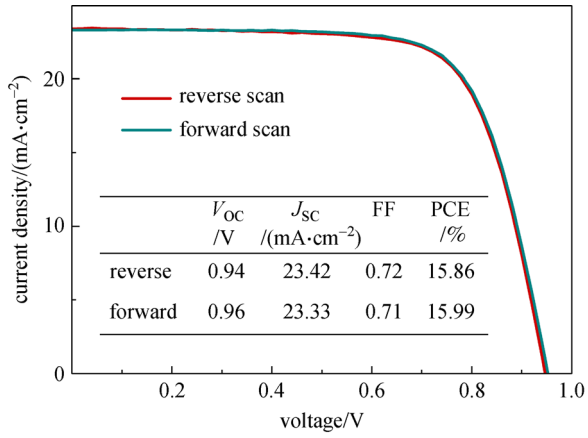

	V_{OC} /V	J_{SC} /(mA·cm^{-2})	FF	PCE /%
reverse	0.94	23.42	0.72	15.86
forward	0.96	23.33	0.71	15.99

Fig. 6 Reverse and forward scan J–V curves of the optimized PMPSC prepared with a precursor at a concentration of 0.70 M

method for the fabrication of printable mesoscopic PSCs. Precursors with lower concentrations were confirmed to result in larger grain sizes due to extended growth time, while higher concentrations led to the development of more continuous films due to sufficient nucleation sites from colloidal particles in the precursor. Among various concentrations from 0.24 to 1.20 M, a moderate concentration of 0.70 M was confirmed to result in the highest PMPSC efficiency of 16.32% due to more effective pore filling and better crystallinity. Furthermore, since the simple drop-coating and spin-coating methods involve different crystallization processes, an efficiency of 15.38% was still achieved at a low concentration of 0.24 M.

Acknowledgements The authors acknowledge financial support from the National Natural Science Foundation of China (Grant Nos. 91733301, 51902117, and 21702069), the Fundamental Research Funds for the Central Universities, the Science and Technology Department of Hubei Province (No. 2017AAA190), the 111 Project (No. B07038), and the Program for Huazhong University of Science and Technology (HUST) Academic Frontier Youth Team (No. 2016QYTD06). We thank the Analytical and Testing Center of HUST for performing various characterization and measurements.

Conflicts of interest There are no conflicts of interest to declare.

References

1. Saliba M, Matsui T, Domanski K, Seo J Y, Ummadisingu A, Zakeeruddin S M, Correa-Baena J P, Tress W R, Abate A, Hagfeldt A, Grätzel M. Incorporation of rubidium cations into perovskite solar cells improves photovoltaic performance. Science, 2016, 354(6309): 206–209
2. Liu S, Guan Y, Sheng Y, Hu Y, Rong Y, Mei A, Han H. A review on additives for halide perovskite solar cells. Advanced Energy Materials, 2020, 10(13): 1902492
3. Stranks S D, Eperon G E, Grancini G, Menelaou C, Alcocer M J P, Leijtens T, Herz L M, Petrozza A, Snaith H J. Electron-hole diffusion lengths exceeding 1 micrometer in an organometal trihalide perovskite absorber. Science, 2013, 342(6156): 341–344
4. Jeon N J, Noh J H, Yang W S, Kim Y C, Ryu S, Seo J, Seok S I. Compositional engineering of perovskite materials for high-performance solar cells. Nature, 2015, 517(7535): 476–480
5. Tong J, Song Z, Kim D H, Chen X, Chen C, Palmstrom A F, Ndione P F, Reese M O, Dunfield S P, Reid O G, Liu J, Zhang F, Harvey S P, Li Z, Christensen S T, Teeter G, Zhao D, Al-Jassim M M, van Hest M F A M, Beard M C, Shaheen S E, Berry J J, Yan Y, Zhu K. Carrier lifetimes of >1 μs in Sn-Pb perovskites enable efficient all-perovskite tandem solar cells. Science, 2019, 364(6439): 475–479
6. Min H, Kim M, Lee S U, Kim H, Kim G, Choi K, Lee J H, Seok S I. Efficient, stable solar cells by using inherent bandgap of α-phase formamidinium lead iodide. Science, 2019, 366(6466): 749–753
7. Kim M, Kim G H, Lee T K, Choi I W, Choi H W, Jo Y, Yoon Y J, Kim J W, Lee J, Huh D, Lee H, Kwak S K, Kim J Y, Kim D S. Methylammonium chloride induces intermediate phase stabilization for efficient perovskite solar cells. Joule, 2019, 3(9): 2179–2192
8. Lin R, Xiao K, Qin Z, Han Q, Zhang C, Wei M, Saidaminov M I, Gao Y, Xu J, Xiao M, Li A, Zhu J, Sargent E H, Tan H. Monolithic all-perovskite tandem solar cells with 24.8% efficiency exploiting comproportionation to suppress Sn(ii) oxidation in precursor ink. Nature Energy, 2019, 4(10): 864–873
9. Nie W, Tsai H, Asadpour R, Blancon J C, Neukirch A J, Gupta G, Crochet J J, Chhowalla M, Tretiak S, Alam M A, Wang H L, Mohite

A D. High-efficiency solution-processed perovskite solar cells with millimeter-scale grains. Science, 2015, 347(6221): 522–525
10. Gong X, Li M, Shi X B, Ma H, Wang Z K, Liao L S. Controllable perovskite crystallization by water additive for high-performance solar cells. Advanced Functional Materials, 2015, 25(42): 6671–6678
11. Bi D, Yi C, Luo J, Décoppet J D, Zhang F, Zakeeruddin S M, Li X, Hagfeldt A, Grätzel M. Polymer-templated nucleation and crystal growth of perovskite films for solar cells with efficiency greater than 21%. Nature Energy, 2016, 1(10): 16142
12. Zhou Y, Game O S, Pang S, Padture N P. Microstructures of organometal trihalide perovskites for solar cells: their evolution from solutions and characterization. Journal of Physical Chemistry Letters, 2015, 6(23): 4827–4839
13. McMeekin D P, Wang Z, Rehman W, Pulvirenti F, Patel J B, Noel N K, Johnston M B, Marder S R, Herz L M, Snaith H J. Crystallization kinetics and morphology control of Formamidinium-Cesium mixed-cation lead mixed-halide perovskite via tunability of the colloidal precursor solution. Advanced Materials, 2017, 29(29): 1607039
14. Nayak P K, Moore D T, Wenger B, Nayak S, Haghighirad A A, Fineberg A, Noel N K, Reid O G, Rumbles G, Kukura P, Vincent K A, Snaith H J. Mechanism for rapid growth of organic-inorganic halide perovskite crystals. Nature Communications, 2016, 7(1): 13303
15. Noel N K, Congiu M, Ramadan A J, Fearn S, McMeekin D P, Patel J B, Johnston M B, Wenger B, Snaith H J. Unveiling the Influence of pH on the crystallization of hybrid perovskites, delivering low voltage loss photovoltaics. Joule, 2017, 1(2): 328–343
16. Etgar L, Gao P, Xue Z, Peng Q, Chandiran A K, Liu B, Nazeeruddin M K, Grätzel M. Mesoscopic $CH_3NH_3PbI_3/TiO_2$ heterojunction solar cells. Journal of the American Chemical Society, 2012, 134(42): 17396–17399
17. Jeon N J, Noh J H, Kim Y C, Yang W S, Ryu S, Seok S I. Solvent engineering for high-performance inorganic-organic hybrid perovskite solar cells. Nature Materials, 2014, 13(9): 897–903
18. Chen J, Xiong Y, Rong Y, Mei A, Sheng Y, Jiang P, Hu Y, Li X, Han H. Solvent effect on the hole-conductor-free fully printable perovskite solar cells. Nano Energy, 2016, 27(Supplement C): 130–137
19. Yan K, Long M, Zhang T, Wei Z, Chen H, Yang S, Xu J. Hybrid halide perovskite solar cell precursors: colloidal chemistry and coordination engineering behind device processing for high efficiency. Journal of the American Chemical Society, 2015, 137(13): 4460–4468
20. Burschka J, Pellet N, Moon S J, Humphry-Baker R, Gao P, Nazeeruddin M K, Grätzel M. Sequential deposition as a route to high-performance perovskite-sensitized solar cells. Nature, 2013, 499(7458): 316–319
21. Bi D, El-Zohry A M, Hagfeldt A, Boschloo G. Unraveling the effect of PbI_2 concentration on charge recombination kinetics in perovskite solar cells. ACS Photonics, 2015, 2(5): 589–594
22. Zhang H, Mao J, He H, Zhang D, Zhu H L, Xie F, Wong K S, Grätzel M, Choy W C H. A smooth $CH_3NH_3PbI_3$ film via a new approach for forming the PbI_2 nanostructure together with strategically high CH_3NH_3I concentration for high efficient planar-heterojunction solar cells. Advanced Energy Materials, 2015, 5(23): 1501354
23. Wieghold S, Correa-Baena J P, Nienhaus L, Sun S, Shulenberger K E, Liu Z, Tresback J S, Shin S S, Bawendi M G, Buonassisi T. Precursor concentration affects grain size, crystal orientation, and local performance in mixed-ion lead perovskite solar cells. ACS Applied Energy Materials, 2018, 1(12): 6801–6808
24. Ku Z, Rong Y, Xu M, Liu T, Han H. Full printable processed mesoscopic $CH_3NH_3PbI_3/TiO_2$ heterojunction solar cells with carbon counter electrode. Scientific Reports, 2013, 3(1): 3132
25. Tian C, Mei A, Zhang S, Tian H, Liu S, Qin F, Xiong Y, Rong Y, Hu Y, Zhou Y, Xie S, Han H. Oxygen management in carbon electrode for high-performance printable perovskite solar cells. Nano Energy, 2018, 53: 160–167
26. Mei A, Li X, Liu L, Ku Z, Liu T, Rong Y, Xu M, Hu M, Chen J, Yang Y, Grätzel M, Han H. A hole-conductor-free, fully printable mesoscopic perovskite solar cell with high stability. Science, 2014, 345(6194): 295–298
27. Rong Y, Hu Y, Mei A, Tan H, Saidaminov M I, Seok S I, McGehee M D, Sargent E H, Han H. Challenges for commercializing perovskite solar cells. Science, 2018, 361(6408): eaat8235
28. Ming Y, Xu M, Liu S, Li D, Wang Q, Hou X, Hu Y, Rong Y, Han H. Ethanol stabilized precursors for highly reproducible printable mesoscopic perovskite solar cells. Journal of Power Sources, 2019, 424: 261–267
29. Rong Y, Hu Y, Ravishankar S, Liu H, Hou X, Sheng Y, Mei A, Wang Q, Li D, Xu M, Bisquert J, Han H. Tunable hysteresis effect for perovskite solar cells. Energy & Environmental Science, 2017, 10(11): 2383–2391
30. Snaith H J, Abate A, Ball J M, Eperon G E, Leijtens T, Noel N K, Stranks S D, Wang J T, Wojciechowski K, Zhang W. Anomalous hysteresis in perovskite solar cells. Journal of Physical Chemistry Letters, 2014, 5(9): 1511–1515

Shuangquan Jiang is a master degree candidate in Optics Engineering at Wuhan National Laboratory for Optoelectronics (WNLO), Huazhong University of Science and Technology (HUST), China. He received his B.Sc. degree in Materials Science and Engineering from Xiangtan University, China in 2017. His current research interest is printable mesoscopic perovskite solar cells.

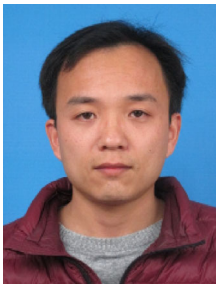

Yusong Sheng is a postdoctoral fellow in the group of Prof. Hongwei Han at Huazhong University of Science and Technology (HUST), China. He received his Ph.D. degree in Optical Engineering (2018) from HUST, China. His current research focuses on the mixed hybrid perovskite materials and stability of printable mesoscopic perovskite solar cell.

Yue Hu is an Associate Professor at Wuhan National Laboratory for Optoelectronics (WNLO), Huazhong University of Science and Technology (HUST), China. She got her B.Sc. degree in Applied Chemistry from East China University of Science and Technology, China and completed her Ph.D. degree in Chemistry in 2016 under the guidance of Prof. Neil Robertson at The University of Edinburgh, UK. She joined HUST, China in 2016 and was promoted to Associate Professor in 2018. Her current research focuses on the designing and synthesizing novel photoactive materials for photovoltaics. She had published more than 50 scientific papers. She was honored a Fraser and Stoddart Prize in 2017.

Yaoguang Rong is an Associate Professor at Wuhan National Laboratory for Optoelectronics (WNLO), Huazhong University of Science and Technology (HUST), China. He received his B.Sc. degree in Material Physics from Wuhan University, China in 2009, and Ph.D. degree in Optics Engineering from HUST, China in 2014. He then worked as a postdoctoral researcher at University of Houston, USA. In 2016, he joined WNLO/HUST, China. His main research interests include perovskite solar cells, dye-sensitized solar cells, and mesoscopic structure materials.

Anyi Mei is an Associate Professor at Wuhan National Laboratory for Optoelectronics (WNLO), Huazhong University of Science and Technology (HUST), China. He received his B.E. degree in Materials Science and Engineering (2013) and Ph.D. degree in Optical Engineering (2018) from HUST, China. His current research interests are focused on printable mesoscopic perovskite solar cells and related materials.

Hongwei Han is a Professor at Wuhan National Laboratory for Optoelectronics (WNLO), Huazhong University of Science and Technology (HUST), China. He received his B.Sc. degree in Applied Chemistry and Ph.D. degree in Condensed Matter Physics from Wuhan University, China in 2000 and 2005, respectively. Later, he stayed in Wuhan University as a lecturer. And then he worked as a postdoctoral research fellow at Monash University in Australia for two years. In 2008, he joined WNLO/HUST, China. His research interests are printable photovoltaics & optoelectronics, especially printable mesoscopic solar cells.